Limits of the Efficiency of Imaging with Obstructing Apertures

A.T. Mohammed

Department of Astronomy, College of Science, University of Baghdad, Jadiria, Iraq, Email: arobie33@yahoo.com.

:
.

.

.   0.6

ABSTRACT: Two-dimensional numerical solutions are carried out to asses the quality of obstructing apertures in terms of the diffraction limited resolution. This include the quality of the point spread function (*psf*), the modulation transfer function (*MTF*), and an image of double lines. These are average intensity of the *psf* (*AI*), maximum intensity of the *psf,(MI)*, full width at half maximum of the *psf* (*FW*) average frequency components of *MTF* (*AFC*), and average side loops of an image of a double lines. The results indicate that the separation of the two lines becomes recognizable using central obstruction of radius equal to or greater than approximately 0.6 times the radius of the primary aperture.

KEYWORDS: Obstructing apertures, optical systems, resolution, fourier transform, image quality.

1. Introduction

All telescopes have an inherent limitation to their angular resolution due to the diffraction of light at the telescope aperture. The diffraction causes an optical system to behave as a low-pass filter in the formation of an image. The cut-off frequency is directly determined by the shape and size of the limiting pupil in the optical system. The incoming light is approximately a plane wave since the source of the light is so far away.

There are several criteria for analyzing the performance of an optical imaging systems. The Rayleigh criterion is generally regarded as a fundamental limit in predicting the performance of optical imaging systems.

According to the Rayleigh criterion, the theoretical resolving power of 5 m optical telescope (λ=400 nm) are $\cong 0.02''$. This value shows the relationship between the resolving power and the telescope apertures. In addition to that criterion, measurements of *MTF*, strehl ratio, and diffraction limited resolution are also very well

considered in quantifying optical systems (William and Bucklund 1989, Harvey and Ftaclas 1995, Brummelaar and Bagnuolo 1995, Brammelaar *et al*. 1994, Baldwin *et al*. 2001, Granieri *et al*. 1998, Jean-Marc *et al*. 2004, Mohammed *et al*. 1990, Milanfar and Shakouri, 2002).

Many studies have been presented in the literatures concerning imaging with obstructing aperture (Fienup 2000, Mohammed 2006, Chakraborty and Thompson 2005).

The aim of this paper is to present the quantitative assessment of the limitations imposed by obstructing apertures on the *psf* and *MTF* in order to determine the constraints on the efficiency of imaging with such apertures.

2.   Theory

The fundamental equation to be used for the formation of an image by an ideal optical system is given by:

$$i(x,y) = \iint_{-\infty}^{\infty} o(x',y') psf(x-x',y-y') dx' dy' \tag{1}$$

$$i(x,y) = o(x,y) \otimes psf(x,y) \tag{2}$$

Equations (1) and (2) are equivalent and representing a convolution equation. Where $i(x,y)$ is the observed image intensity, $o(x,y)$ is the object intensity, $psf(x,y)$ represents the image blurring function caused by the imaging system and $\otimes$ denotes convolution operator.

The Fourier transform of (2) is given by:

$$I(u,v) = O(u,v). T(u,v) \tag{3}$$

where $I(u,v)$ and $O(u,v)$ are, respectively, the complex Fourier transforms of the image intensity $i(x,y)$, and the object intensity $o(x,y)$; $T(u,v)$ which represents the Fourier transform of the *psf*, is an important function known as the optical transfer function (*OTF*). The modulation or amplitude of the complex function $T(u,v)$ is called *MTF*. In general, the resolution of an imaging system is limited only by the luck of large optical elements that are free from inherent distortions.

Now consider an extremely distant quasimonochromatic point source located on the optical axis of a simple imaging system. In the absence of atmospheric turbulence, this source would generate a plane wave normally incident on the lens. In the presence of the atmosphere, the plane wave incident on the inhomogeneous medium propagates into the medium, and ultimately a perturbed wave falls on the lens. The field distribution incident on the lens can be expressed as,

$$U(\eta,\gamma) = e^{i\phi(\eta,\gamma)} \tag{4}$$

where $\phi(\eta,\gamma)$ is the random phase of the incident wavefront and the variables (η,γ) represent distances in the pupil function. The instantaneous *psf* of the entire telescope atmosphere system is given by:

$$psf(x,y) = \left| FT[H(\eta,\gamma) U(\eta,\gamma)] \right|^2 \tag{5}$$

(a)   (b)
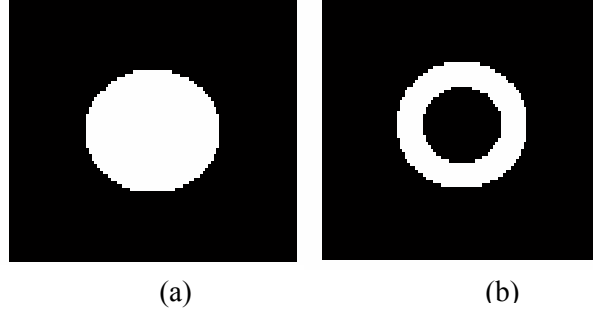
Figure 1. Telescope apertures:(a) Uniform ($\varepsilon = 0$), (b) $\varepsilon = 0.6$

where $H_{(\eta,\gamma)}$ represents the pupil function and *FT* denotes *Fourier transform* operator. The corresponding *OTF* is the *Fourier transform* of the *psf*, thus

$$T(u, v) = FT[psf(x, y)] \tag{6}$$

Equation (6) can also be written in terms of the pupil function and the field distribution incident on the lens as,

$$T(u,v) = \iint_{-\infty}^{\infty} H(\eta,\gamma)H*(\eta-\eta',\gamma-\gamma').$$
$$U(\eta,\gamma)U*(\eta-\eta',\gamma-\gamma')d\eta'd\gamma' \tag{7}$$

where * denotes complex conjugate. The variables η and γ are related to the Fourier space variables u and v by $\eta = \lambda f u$, $\gamma = \lambda f \upsilon$, where λ is the wavelength and f is the focal length.

3. Simulations

The size of the pupil function $H(u,y)$ is taken to be a two dimensional circular function of radius R and of unity magnitude; this array $(M \times N)$ is of size 512×512 pixels. This size is taken as large as possible in order to keep the theoretical diffraction limiting resolution vanishing to zero inside this array. This aperture is said to be a uniform aperture.

The central obstructing aperture is simulated by calculating the parameter ε. This parameter represents the ratio of the radius of obstructing circle (r) to the radius of the uniform aperture, R, i.e., $\varepsilon = r/R$.
Telescope apertures of $\varepsilon = 0$ and $\varepsilon = 0.6$ are demonstrated   in Figure 1.

We consider the object to be imaged is   an extremely distant quasimonochromatic point source located on the axis of an optical telescope. In the absence of atmospheric turbulence, this source would generates a plane wave $\left[\phi(\eta,\gamma) = 0 \text{ and } U(\eta,\gamma) = 1\right]$.

The *psfs* are computed via Equation (5). The perspective plots of the central regions of these *psfs* (14 pixels by 14 pixels) are shown in Figure 2.
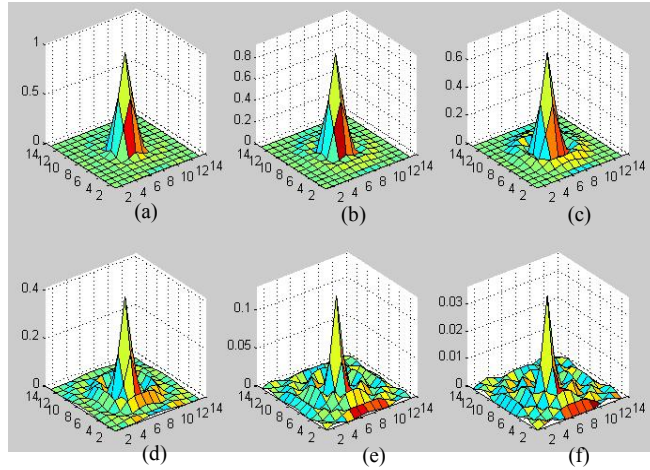
Figure 2. Perspective plots of the central regions of psf's, (a) Uniform aperture,(b) $\varepsilon = 0.2$,(c) $\varepsilon = 0.4$, (d) $\varepsilon = 0.6$ and (e) $\varepsilon = 0.8$ (f) $\varepsilon = 0.9$.

It should be pointed out here that the central spikes of the *psfs* are very sharp. This is because *R* is taken to be very large, *R=120* pixels.
The line plots through the centre of these regions are shown in Figure 3.
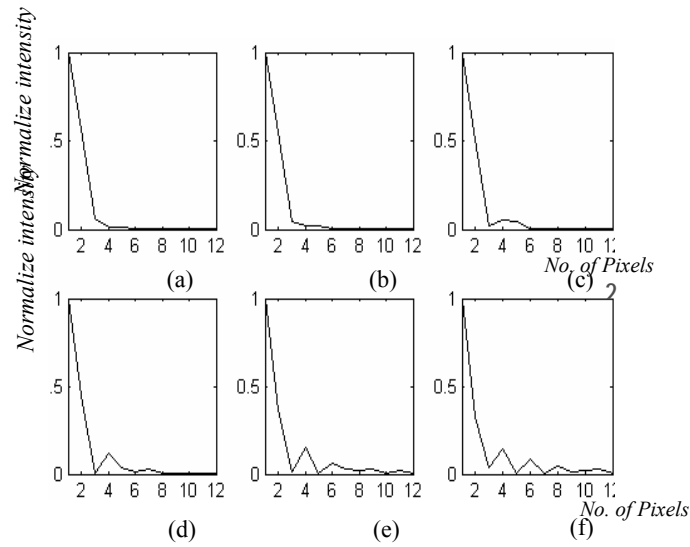
Figure 3. Plots through the central regions of the psfs. (a) Uniform aperture,(b) $\varepsilon = 0.2$,(c) $\varepsilon = 0.4$,(d) $\varepsilon = 0.6$,(e) $\varepsilon = 0.8$ and (f) $\varepsilon = 0.9$.

The *MTFs* are also computed according to Equation (6) or (7) respectively and absolute values are taken for *T(u,v)*. The results are shown in Figure 4.

(a)   (b)   (c)

(d)   (e)   (f)
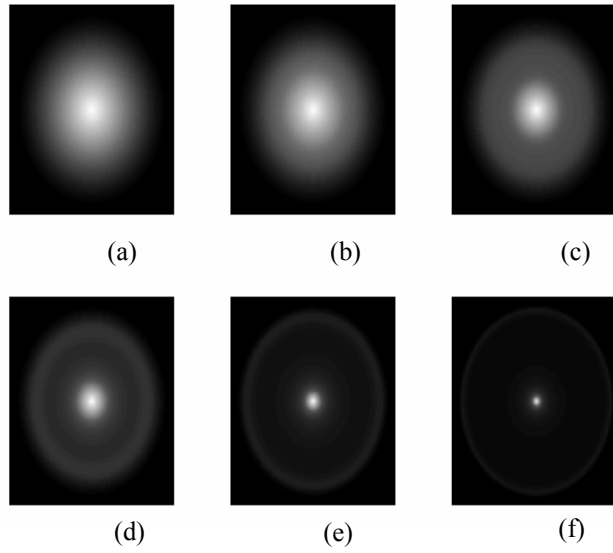
Figure 4. MTF's (a) Uniform aperture,(b) $\varepsilon = 0.2$,(c) $\varepsilon = 0.4$,(d) $\varepsilon = 0.6$ (e) $\varepsilon = 0.8$ and (f) $\varepsilon = 0.9$

The above images are then normalized to their maximum values according to the following equation:

$$MTF_N(x,y) = \frac{MTF(x,y)}{MTF(0,0)} \qquad (8)$$
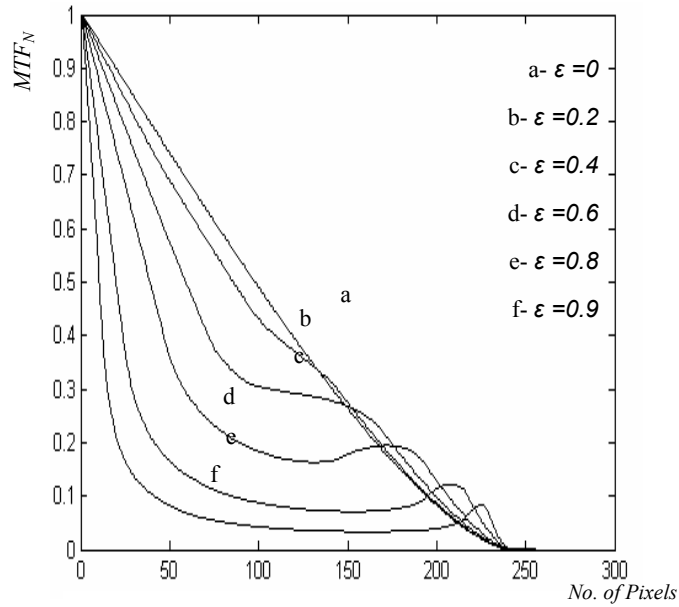
Figure 5. Central plots through Figure 4.

where $MTF(0,0)$ represents the value of the central spike.
The central lines of the normalized $MTFs$ (i.e. MTF_N) are plotted in Figure 5.

71

The *psfs* at different values of ε are convolved with the double line object presented in Figure 6(a). The lines are one pixel wide separated by a distance of 2 pixels. This value is chosen because the full width of the *psf* of the uniform aperture is 3 pixels. The results are shown in Figure 6.
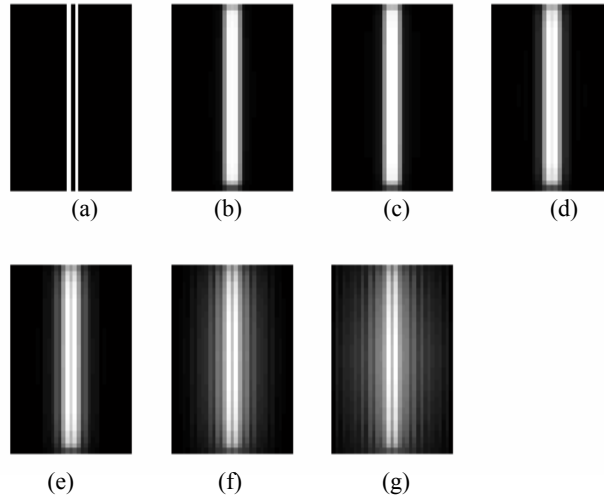
Figure 6. Line Convolutions:(a) Uniform aperture, (b) $\varepsilon = 0.2$, (c) $\varepsilon = 0.4$, (d) $\varepsilon = 0.6$, (e) $\varepsilon = 0.8$ and (f) $\varepsilon = 0.9$.

The images in Figure 6 are then normalized to one at their maximum values and the central lines through these images are plotted. The results are presented in Figure 7.
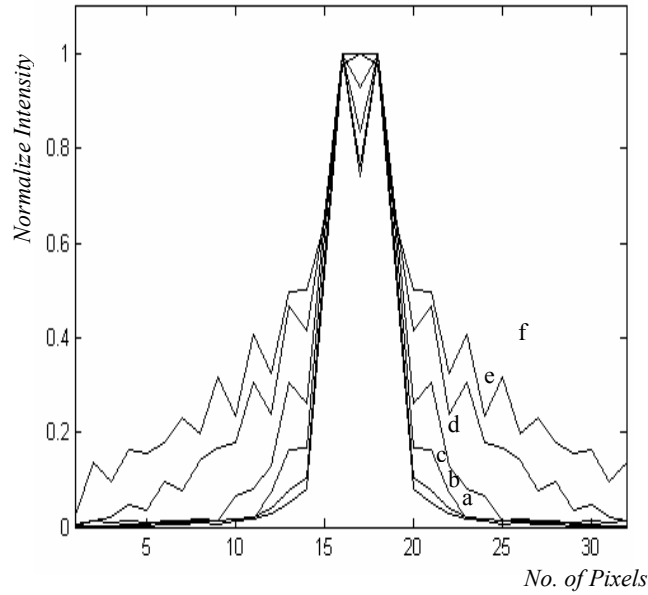
Figure 7. Normalized Intensities through the center of the images in Figure 6. (a) Uniform aperture,(b)$\varepsilon = 0.2$,(c) $\varepsilon = 0.4$,(d) $\varepsilon = 0.6$,(e) $\varepsilon = 0.8$ and (f) $\varepsilon = 0.9$.

For $\varepsilon = 0$, the line plot shows a little peak at the center. As ε increases, the separation of the double lines becomes recognizable and the side loops become severe.

The normalized maximum intensity values (*MI*) of the *psfs* are calculated and presented in the Table 1 given below as follows. First, the maximum value of the *psf* of the uniform aperture ($\varepsilon = 0$) is calculated. Secondly, the maximum intensity values at different ε are divided by the maximum value at $\varepsilon = 0$.
This measure is taken in order to examine the dropness in the value of the central spike of the *psf* as a function of ε.

Table 1. The variation of MI, AI, FW, AFC and SL at different values of ε.

ε	MI	AI	FW	AFC	SL
0	1	1	3	1	1
0.2	0.9224	1.0412	3	0.9604	1.0808
0.4	0.707	1.19	3	0.8406	1.2373
0.6	0.411	1.56	1	0.6410	1.5328
0.8	0.13	2.77	1	0.3607	2.3403
0.9	0.0362	5.26	1	0.1902	3.0122

The average intensity values (*AI*) of the *psf* at different ε is computed by:

$$\mathrm{A}I = \sum_{y=1}^{M}\sum_{x=1}^{N} psf(x,y) \Bigg/ \sum_{y=1}^{M}\sum_{x=1}^{N} psf_U(\mathrm{x,y}) \qquad (9)$$

where $psf_U(x,y)$ *is the psf at* $\varepsilon =0$.
The average frequency components (*AFC*) of *MTF* (*u,v*) at different ε are computed by:

$$\mathrm{AFC} = \sum_{u=1}^{M}\sum_{v=1}^{N}\mathrm{MTF}(u,v) \Bigg/ \sum_{u=1}^{M}\sum_{v=1}^{N} MTF_U(u,v) \qquad (10)$$

where $MTF_U(u,v)$ *is the MTF at* $\varepsilon =0$.

The full width of the *psf* (*FW*) at different ε are also calculated and presented in this table. These values indicate the width of the central spike of the *psfs*.

The summation of all values that located outside the double lines of the *psfs* at different ε (see Figure.6) are computed and the values are then divided by the corresponding value of the uniform aperture. The results are describing the actual weight of the side loops (*SL*).

4. Conclusions

The following conclusions could be drawn :
1. The *MI* value decreases by a factor of $\cong 30$ as ε goes from $\varepsilon = 0$ to $\varepsilon = 0.9$. This great reduction in the height of central spike will enhance the probability of detecting faint companion (Figure 7 describes normalized intensity not actual intensity).
2. As ε increases, *AI* increases and at $\varepsilon = 0.9$, *AI* increases by a factor of $\cong 5$. This is of course will create artifacts in the observed images (see Figure. 2).
3. *FW* reduced dramatically as ε increases. For $\varepsilon = 0.6$, *FW* reduces by a factor of 3. This will enhance the resolution by a factor of 3.

73

4. *AFC* reduces by nearly a factor of $\cong 5$ at $\varepsilon = 0.9$. This is because the build up of the side loops in the *psfs*. *AFC* is inversely proportional to ε.
5. The *SL* increases by a factor of 3 at $\varepsilon = 0.9$. *SL* is linearly proportional to ε.

6. References

BALDWIN, J.E., TUBBS, R.N., COX, G.C., MACKAY, C.D., WILSON, R.W. and ANDERSON, M.I. 2001. Diffraction limited 800 nm imaging with 2.56 m Nordic optical telescope. *Astronomy and Astrophysics* **368:** L1-L4.

BRUMMELAAR, T.A. and BAGNUOLO, W.G. 1995. Strehl ratio and visibility in long baseline stellar interferometry. *Optics Letters* **20:** 521-23.

BRUMMELAAR, T.A., BAGNUOLO, W.G. and RIDGWAY, S.T. 1994. Strehl ratio and coherence loss in long baseline interferometry. *Technical Report, Center for High Angular Resolution Astronomy Georgia State University*, No. 6.

CHAKRABORTY, A. and THOMPSON, L.A. 2005. 10^{-7} contrast ratio at $4.5\lambda/D$:New results obtained in laboratory experiments using nonfabricated coronograph and multi-Gaussian shaped pupil masks. *Optics express* **13:** 2394.

DEBES, J. 2003. High contrast imaging with Gaussian aperture pupil mask. *astro-ph 0301051, V* **1**.

FIENUP, J.R. 2000. MTF and integration time versus fill factor for sparse-aperture imaging system. *Proc. SPIE*. 4091 A-06 San Diego, CA.

GRANIERI, S., ENRIQUE, E. and FURLAN, W.D. 1998. Performance analysis of optical imaging systems based on fractional Fourier transform. *Journal of Modern Optics* **45:** 1797-07.

HARVEY, J.E and FTACLAS, C. 1995. Diffraction effects of telescope secondary mirror spiders on various image quality criteria. *Applied Optics* **34:** 6337-49.

JEAN-MARC, D., LEGER, D., ROGUES, S. and VALORGE, C. 2004. Modulation transfer function estimation from non specific images. Optical Engineering **43:** 1355-65 DONAL, F.O'shea; Ed.

MILANFAR, P. and SHAKOURI, A. 2002. Statistical analysis of diffraction limited images. *IEEE ICIP*.

MOHAMMED, A.T., RASHID, N.M. and SADIK, A.R. 1990. Computer simulations of astronomical objects as seen by ground based optical telescope. *Optics and Lasers in Engineering* **12:** 223-43.

MOHAMMED, A.T. 2006. Quantitative analysis of imaging with apodized square apertures. *Iraqi Journal of Science* **47:** 255-61.

SONG, JONG.SUP., LEE YUN WOO, SONG JAE BONG, LEE IN WON, YANG HO-SOON, CHOI YOUNG-WAN, and DUAL JAE HEUNGO JO. 2002. Dual testing of a large aperture optical system. *Proc. SPIE, Interferometry XI:Applications*, **4778:** 227-36.

WILLIAM, C. and BECKLUND, O. 1989. *Introduction to the Optical Transfer Function.* Wiley Series in Pure and Applied Optics.